INTERFACE FOCUS

rsfs.royalsocietypublishing.org

Research

Cite this article: De Sanctis A, Russo S, Craciun MF, Alexeev A, Barnes MD, Nagareddy VK, Wright CD. 2018 New routes to the functionalization patterning and manufacture of graphene-based materials for biomedical applications. *Interface Focus* **8**: 20170057. http://dx.doi.org/10.1098/rsfs.2017.0057

Accepted: 31 January 2018

One contribution of 13 to a theme issue 'The biomedical applications of graphene'.

Subject Areas:
biomaterials, biophysics, nanotechnology

Keywords:
graphene, biomedical applications, graphene functionalization

Author for correspondence:
C. D. Wright
e-mail: david.wright@exeter.ac.uk

New routes to the functionalization patterning and manufacture of graphene-based materials for biomedical applications

A. De Sanctis, S. Russo, M. F. Craciun, A. Alexeev, M. D. Barnes, V. K. Nagareddy and C. D. Wright

Centre for Graphene Science, College of Engineering, Mathematics and Physical Sciences, University of Exeter, Exeter EX4 4QF, UK

CDW, 0000-0003-4087-7467

Graphene-based materials are being widely explored for a range of biomedical applications, from targeted drug delivery to biosensing, bioimaging and use for antibacterial treatments, to name but a few. In many such applications, it is not graphene itself that is used as the active agent, but one of its chemically functionalized forms. The type of chemical species used for functionalization will play a key role in determining the utility of any graphene-based device in any particular biomedical application, because this determines to a large part its physical, chemical, electrical and optical interactions. However, other factors will also be important in determining the eventual uptake of graphene-based biomedical technologies, in particular the ease and cost of manufacture of proposed device and system designs. In this work, we describe three novel routes for the chemical functionalization of graphene using oxygen, iron chloride and fluorine. We also introduce novel *in situ* methods for controlling and patterning such functionalization on the micro- and nanoscales. Our approaches are readily transferable to large-scale manufacturing, potentially paving the way for the eventual cost-effective production of functionalized graphene-based materials, devices and systems for a range of important biomedical applications.

1. Introduction

The biomedical applications of graphene-based materials are wide-ranging and potentially of much importance and impact, spanning, for example, drug delivery, photothermal therapy, tissue engineering, bactericides, biosensing and bioimaging [1]. Such wide-ranging applicability of graphene arises from its unique physical, electrical, mechanical and chemical properties, in particular its high surface area, excellent electrical and thermal conductivity, optical transparency, biocompatibility and, importantly, its ease of functionalization. Indeed, for many biomedical applications it is not graphene *per se* that is used as the active material, but rather a functionalized form of graphene, where functionalization with particular chemical species has been carried out in order to enhance performance and increase selectivity (e.g. to a particular reaction).

One of the most widely used functionalization routes is that leading to the formation of graphene oxide (GO), where oxygen-bearing groups functionalize the graphene, forming mainly epoxide (C−O−C), hydroxyl (C−OH), carbonyl (C=O) and carboxyl (O−C=OH) bonds. GO (and reduced GO) has been used extensively for drug delivery in cancer treatment (e.g. [2–4]), for the fabrication of biosensing platforms capable of detecting the presence of key disease biomarkers and DNA sequences (e.g. [5–7]), for the *in situ* bioimaging of cells [8], as well as finding application as a most effective antibacterial agent (e.g. [9–11]). Oxygen is, however, not the only useful species for graphene functionalization, far from it. Indeed, a wide variety of functionalization routes have

THE ROYAL SOCIETY PUBLISHING

been investigated using organic and inorganic species and covalent and non-covalent approaches (e.g. [12]). We ourselves, for example, have shown that functionalization of few-layer graphene (FLG) with iron chloride ($FeCl_3$) leads to exceptional photoelectrical properties [13] that can be exploited in a wide variety of applications, including highly sensitive and high-resolution photodetectors for biosensing and bioimaging. Fluorine-functionalized graphene has also been shown to possess very useful biomedical applications, particularly for the detection of various analytes and biomarkers [14], and may ultimately find application in the management and detection of a range of important and widespread health problems, such as diabetes and cardiovascular disease.

In this study, we report on the functionalization of graphene using the three chemical species introduced above, namely oxygen, iron chloride and fluorine. In particular, we report on novel ways for localizing such functionalization, potentially down to the nanoscale. The ability to exert local control of the functionalization process and to pattern functionalized regions as desired in a simple and effective way, which we demonstrate here, should make for more straightforward and cost-effective production of future graphene-based biomedical devices.

2. New routes to oxygen-functionalized graphene devices

The efficient and cost-effective production of functionalized graphene devices is still hampered somewhat by conventional approaches to device fabrication. Such conventional approaches involve several process steps including graphene deposition, graphene film transfer, graphene functionalization, *ex situ* lithographic patterning and metal contact deposition; processes that are time-consuming, not always reproducible and potentially deleterious to the properties of the chemical vapour deposition (CVD) graphene layer itself (e.g. [15–17]). An alternative approach that avoids many such drawbacks is to carry out *in situ* plasma functionalization and *in situ* lithographic patterning of large-area CVD graphene directly on the copper substrates used in the graphene deposition process. This enables the fabrication of devices in their entirety prior to any transfer steps. Here we concentrate on the production of oxygen (plasma) functionalized graphene materials and devices which, as discussed in the introduction above, have found widespread application in the biomedical field.

The plasma oxidation method for the production of GO has several advantages compared to the more commonly used liquid-phase approaches (such as the Hummers method). In particular, plasma oxidation does not contaminate samples with by-products of (wet) chemical reactions [18,19], it is easily scaled in size, is relatively environment-friendly and involves fewer stages when compared with conventional methods [20]. Moreover, patterned graphene/GO structures and devices can also be readily created using plasma modification of graphene combined with lithographic processing, and this can all be carried out prior to the transfer, onto the desired substrate, of the (functionalized and patterned) graphene from its CVD (catalytic) Cu foils [21]. In this way complex micro- and nanoscale GO device structures can be reliably fabricated in fewer steps than via conventional approaches and, importantly, be readily transferred onto a range of target surfaces including rigid and flexible substrates, biocompatible substrates and even textiles (e.g. for wearable biomedical devices).

Our fabrication process is illustrated in figure 1, here using an 80×80 μm GO logo (a G surrounded by an O) by way of demonstration (and in which the G and O regions are plasma-oxidized, while the remainder of the film remains as graphene). In detail, our process is as follows: first, a 200 nm thick layer of positive e-beam resist (poly(methyl methacrylate), PMMA) is spin-coated onto graphene film on copper foil, as grown by the CVD method; next, the area to be functionalized is exposed by the e-beam and subsequently developed, leaving the unmasked regions of the graphene film exposed; next the sample is exposed to the oxygen plasma; then, the copper substrate is etched away from the underside using ammonium persulfate solution; the PMMA–graphene stack is cleaned multiple times in de-ionized water and then transferred onto the target substrate; finally, the PMMA mask is removed using acetone and the sample is cleaned with isopropyl alcohol. To verify that the G and O patterned regions, and only those regions, were successfully oxidized, we carried out Raman mapping of the sample (with a 1 μm step size) and plot, in figure 1*g*, the ratio of the intensities of the Raman D and G peaks (I_D/I_G). It can be seen that a striking I_D/I_G contrast exists between the oxidized regions and those that were protected from the plasma, indicating successful oxidation of the desired regions. The oxidized 'GO logo' pattern of figure 1*g* can also be clearly seen via scanning electron microscopy (SEM) imaging, as shown in figure 1*h*, the darker regions in that image indicating a reduction in the conductivity of the plasma exposed area.

The quality, in terms of overall O content and oxygen-bearing functional groups present, of the plasma functionalized GO produced by the method shown in figure 1 is high (as confirmed by the Raman spectrum, which is essentially the same as it is for GO prepared by standard wet-chemistry methods; see [21]). The homogeneity of the plasma functionalized GO is also high, even in the case of patterned structures. This is due to two main reasons. Firstly, the grains in our CVD-grown graphene are small (significantly sub-micrometric) and evenly distributed, so any preferential oxidation that occurs at grain edges is also evenly distributed. Secondly, the dominant oxygen-bearing group in our plasma-oxidized films is epoxide (C–O–C) which, as is well known (e.g. [22]), does not need edges to form.

Although we have here shown the production of a simple logo to demonstrate on the micrometre scale the effective local functionalization of graphene (to GO), it is straightforward to use the technique we have presented to fabricate entire devices with features down to the nanoscale if desired. For example, we have previously successfully produced a flexible and transparent plasma functionalized graphene/GO humidity sensor that outperformed high-grade commercial humidity sensors [21]. The production of biomedical-oriented devices using our technique is also entirely feasible and could prove particularly beneficial in the biosensing area. Moreover, while we in this section have concentrated on oxygen plasma functionalization, the approach described is generic and can undoubtedly be applied in the case of functionalization by other chemical species.

3. New routes to patterning $FeCl_3$-functionalized graphene for high-definition bioimaging and biosensing

Optoelectronic biosensing platforms are attracting growing interest as they can potentially be incorporated in portable

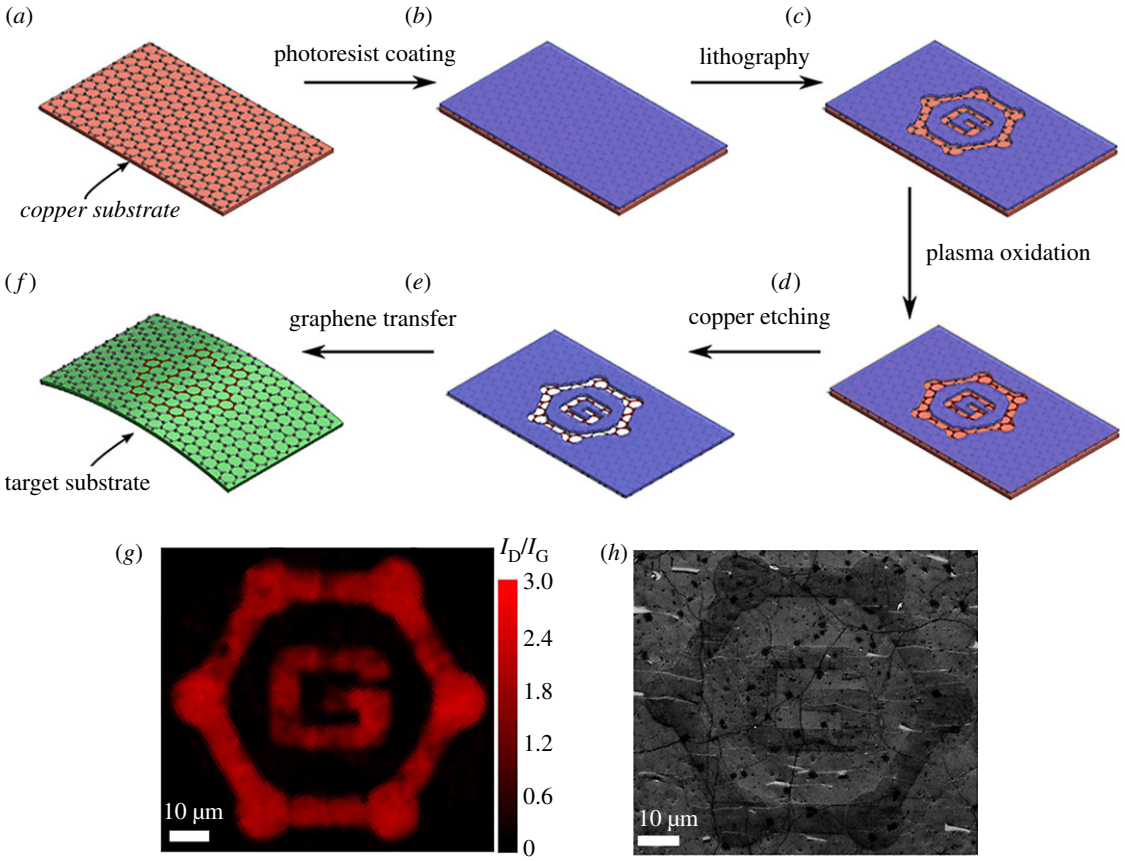

Figure 1. Schematic of the *in situ* functionalization (here using oxygen) and patterning of as-grown CVD graphene: (*a*) to (*b*) photoresist (PMMA) coating of as-grown CVD graphene; (*b*) to (*c*) e-beam lithography on Cu; (*c*) to (*d*) plasma oxidation (in a reactive ion etching system); (*d*) to (*e*) copper etching in ammonium persulfate solution; (*e*) to (*f*) graphene transfer onto the target (here shown as a flexible) substrate; (*g*) and (*h*) show a Raman I_D/I_G map and SEM image of the final 80 × 80 μm GO logo. (Adapted and reprinted with permission from Alexeev *et al*. [21]. (Copyright 2016 IoP.) (Online version in colour.)

medical devices to be used in a multiplicity of environments [23]. In general, such platforms are based on a light source, a reactive medium and a photodetector with spectral selectivity. Thus, photodetectors for high-definition sensing and imaging and able to operate in various spectral ranges are needed. In particular, infrared (IR) and near-infrared (NIR) detectors have applications in biochemical detection and functional-NIR medical imaging. On the other hand, ultraviolet (UV) light is strongly absorbed by many materials, enabling the observation of characteristics that are difficult to detect by other methods. For example, UV imaging is an emerging inspection method for microbial contamination of food products. Several alternative approaches for optoelectronic biosensing have been demonstrated in recent years based, for example, on plasmonic nano-resonators [24], optofluidic devices [25] or integrated semiconductor photodetectors [26,27]. However, the push for the development of low-cost, flexible and wearable devices [28] has instigated the exploration of novel materials, among which is graphene [29,30] and its functionalized forms.

While in the previous section we concentrated on oxygen functionalization, we now turn our attention to the functionalization of FLG with $FeCl_3$. This results in the best transparent electrical conductor currently available [13], and one that outperforms indium tin oxide as currently used extensively in touch screen displays etc. However, $FeCl_3$ functionalized graphene is much more than just a high-performance transparent conductor; it offers a gamut of exciting properties and potential for various applications. Examples include an unforeseen stability to harsh environmental conditions [31], ease of large-area processing [32], the realization of all-graphene photodetectors [32] and the potential to enhance the efficiency of photovoltaic and organic light-emitting devices [32,33]. When used as a transparent electrode in electroluminescent devices, $FeCl_3$-functionalized graphene also increases the brightness of the emitted light by up to 50% when compared with pristine graphene, and up to 30% compared with state-of-the-art commercial electrodes [34]. Furthermore, the record high charge density achieved in $FeCl_3$-functionalized graphene [13,35] makes it an attractive platform for the production of high-responsivity, high-resolution photodetectors.

Graphene-enabled high-resolution imaging could open a new era in small-footprint high-performance biosensing devices. However, the scientific community is presently facing difficult challenges in realizing such devices. In particular, efficient nanoscale graphene photodetectors are presently not possible due to the dominance of photo-thermoelectric effects (PTE) in graphene, which sets the minimum size for a graphene pixel to the tens of micrometres scale (as demonstrated by several pioneering works [36–40]). Another obstacle is imposed by the diffraction limit, setting a further constraint on the (minimum) size of devices. Furthermore, the electrical and optical properties of graphene are severely hampered by contamination of the material in ambient conditions, requiring elaborate ways of encapsulation to preserve the properties of graphene, hence limiting its use in realistic situations [41].

Many of the above issues have been recently tackled using $FeCl_3$-intercalated FLG [13,31–35,42] ($FeCl_3$-FLG), together with a new way to define optically active junctions [43]. As shown in figure 2*a*, a laser beam is used to control the

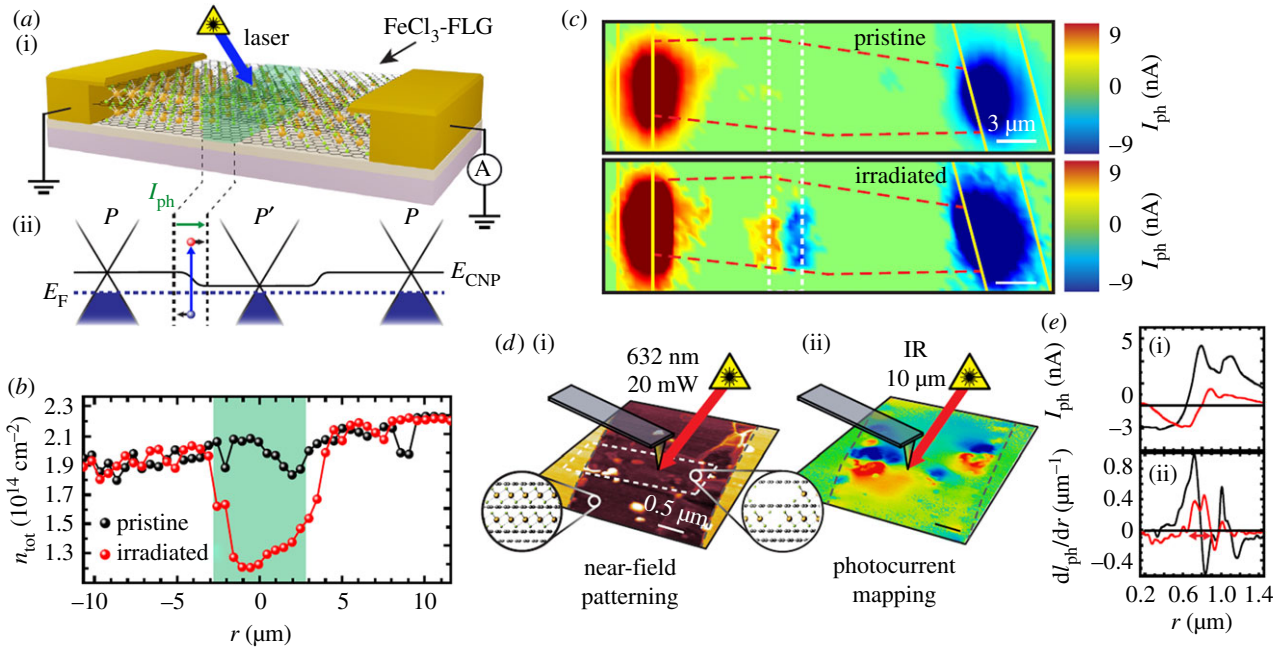

Figure 2. Laser-written photodetectors in $FeCl_3$-intercalated graphene. (*a*) Device structure and scanning photocurrent measurement configuration (i) of a p–p′–p junction. The selective displacement of $FeCl_3$ molecules with laser light allows the formation of a p region (in green). The schematic band structure (ii) of each region illustrates how photogenerated carriers drift under the induced chemical potential gradient. (*b*) Total charge carrier concentration in pristine and laser-irradiated $FeCl_3$-FLG. (*c*) Scanning photocurrent maps of a $FeCl_3$-FLG flake (red-dashed lines) with Au contacts (yellow lines) before and after laser-assisted displacement of $FeCl_3$ (white dashed lines). (*d*) Near-field patterning of photoactive junctions in $FeCl_3$-FLG. AFM topography (i) and scanning photocurrent map (ii) of the flake after laser irradiation by a $\lambda = 632$ nm laser (white dashed lines). Insets: illustrations of the chemical structure in p- and p-doped regions. (*e*) Line scans of photocurrent measured across the laser-defined p–p′–p junctions. (ii) Shows first derivative plots of the photocurrent signal, indicating a peak-to-peak distance of only 250 nm between adjacent junctions. (Adapted and reprinted with permission from De Sanctis *et al*. [43]. Under CC-BY license from AAAS, 2017.) (Online version in colour.)

microscopic arrangement of $FeCl_3$ molecules which are intercalated between sheets of graphene, in order to define photoresponsive junctions. This approach enables conceptually new ways to capture and manipulate light beyond conventional plasmonic structures. Intercalation of graphene with $FeCl_3$ results in a strong charge-transfer [13,32] and consequent p-type doping of the graphene. By selectively removing $FeCl_3$ molecules, therefore, a p–p′ junction can be defined, as shown in figure 2*b* (where the total charge concentration in the graphene stack is shown before and after laser irradiation of a strip across the sample [32,44]). Such a junction shows a strong photoresponse, as shown by the scanning photocurrent maps in figure 2*c*. By analysing the direction of the observed photocurrent and calculating the different contributions to the photocurrent arising from the PTE and photovoltaic (PV) effects, it is shown that in $FeCl_3$-intercalated graphene strong quenching of PTE effects is possible and the photoresponse is dominated by the PV effect [43].

The quenching of the PTE effect in $FeCl_3$-FLG removes one of the key limitations, in terms of device scaling and hence sensing and imaging resolution, of graphene-only photodetectors. Indeed, the quenching of the PTE effect in $FeCl_3$-FLG allows the definition of photoactive junctions in a much more confined space. To this end, emerging nano-photonics near-field techniques [45] can be used in order to surpass the other 'block' on high-resolution sensing and imaging, namely the diffraction limit. For example, in figure 2*d*,*e* a red ($\lambda = 632$ nm) laser focused onto a metallic atomic-force microscope (AFM) tip is used to define a photoactive p–p′ junction with a peak-to-peak distance of only 250 nm, less than half the laser wavelength used. The broad spectral response of graphene is also maintained in these sub-diffraction $FeCl_3$-FLG devices, which show a consistent proportionality between optical response and photon energy from the ultraviolet (UV) right through to mid-infrared wavelengths. Another extraordinary characteristic of laser patterned $FeCl_3$-FLG junctions is their linear dynamic range (LDR). This parameter determines the range of power densities over which a photodetector's response is linear. In graphene such linearity is limited by the aforementioned PTE effect and the small density of states available for photoexcitation. In $FeCl_3$-FLG, instead, an LDR of 44 dB is observed. This is a remarkable 4500 times larger than any other graphene-based photodetector reported to date [43].

To summarize, by using $FeCl_3$ functionalization of graphene, we can 'engineer' the hot carrier photoresponse so as to enhance both pixel resolution and LDR, while at the same time maintaining a broad spectral response, in atomically thin devices and systems. Such capabilities could have potentially wide-reaching impacts on technologies for spectroscopy, high-definition bioimaging and biosensing. We might see their use in, for example, disposable medical diagnostic tools for the detection of biofluorescent molecules with sub-wavelength resolution [46], or in skin-conformable photodetectors for heart rate measurements (known as photoplethysmography), or perhaps wearable and elastic UV cameras for minimally invasive probes and UV tracking.

4. Nano-patterning of fluorine-functionalized graphene for biosensing

Yet another biologically useful functionalization of graphene is that using fluorine. In fluorinated graphene (FG), fluorine

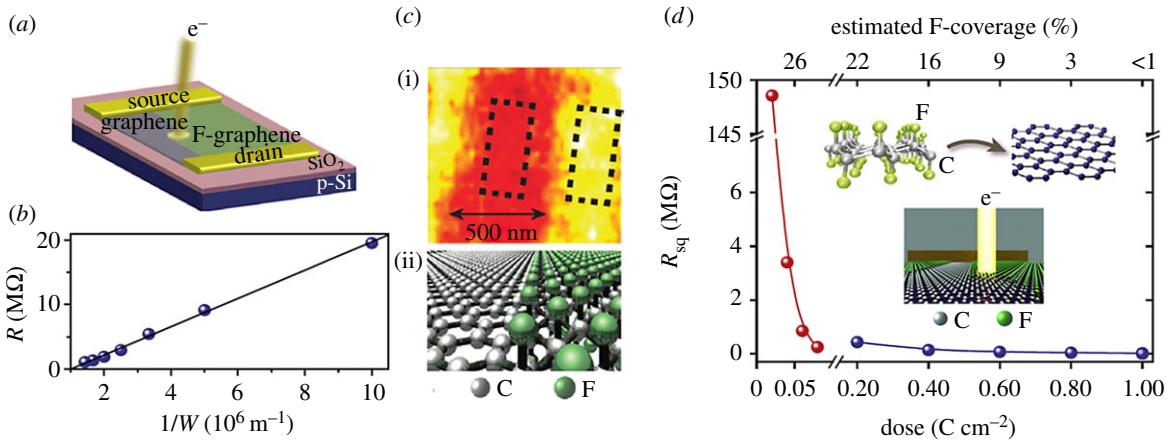

Figure 3. Nano-patterning fluorinated graphene. (*a*) Schematic illustration of the device configuration under irradiation with a beam of electrons. The fluorinated graphene (green) is reduced to graphene (grey) upon electron irradiation. (*b*) The sample resistance plotted against inverse width *W* for a device. The continuous line is a linear fit. (*c*) Topographical AFM image for the unexposed (orange) and exposed (red) fluorinated graphene. (ii) Illustrates the crystal structure of pristine graphene (grey) and fluorinated graphene (green). (Reprinted with permission from Withers *et al*. [54]. Copyright 2011 American Chemical Society.) (*d*) Graph of the measured zero-bias square resistance (Rsq) at room temperature after subsequent steps of electron-assisted defluorination conducted on the same sample. The insets show the process of electron-assisted defluorination where fluorinated graphene (left structure with carbon atoms in grey and fluorine atoms in green) is reduced to graphene (right structure). (Reprinted with permission from Martins *et al*. [55]. Under CC-BY-SA license. Copyright 2013 DPG/IoP.) (Online version in colour.)

adatoms are covalently bonded to the carbon atoms and, owing to the high electronegativity of the bound fluorine, FG benefits from an augmented sensing performance for various analytes and biomarkers [14]. Previous studies have also revealed that sensing activity strongly depends on the fluorine content [47]; the interactions between FG and biomolecules can be drastically modified by varying the amount of fluorine functionalization. For instance, different carbon-to-fluorine ratios have been used to prepare biosensors able to detect ascorbic acid, uric acid [48] and ammonia [49]. Hence controlling and tuning the fluorine content are important aspects for the further development of FG-based biosensors. In particular, the possibility to control locally the fluorine content would enable a new concept of biosensing applications whereby a wide variety of biomolecules can be detected at different positions on the same sensor by patterning the degree of functionalization.

One approach towards such local control of fluorination is similar to the patterning of GO using plasma functionalization, as discussed in §2 above. For example, it has been shown that F-functionalized graphene can be prepared using F-based plasma treatments to provide a highly stable covalent bond of C−F [50–52]. Furthermore, to achieve local fluorination, a patterned buffer layer during the CF_4 plasma treatment has been successfully demonstrated [53].

Another approach to the local control of fluorination is to start from a highly fluorinated graphene sheet and reduce the level of functionalization in specific regions by irradiation with an electron beam [54,55]. This approach is summarized in figure 3. The starting material is a sheet of functionalized graphene obtained by exposure to F_2 gas at 450°C, resulting in a fluorine content of 28%. Subsequently, irradiation of the functionalized graphene with an electron beam with appropriate energy dissociates the C−F bonds, hence reducing the level of fluorination. This innovative technique offers a simple and direct way to pattern spatially, on the nanoscale, the degree of fluorination. This has also been experimentally confirmed by the demonstration that the value of the energy gap of FG depends on the F content. As shown in figure 3*d*, a transition from a wide-gap semiconductor (i.e. FG) to a semi-metal (i.e. graphene) was experimentally observed upon changing *in situ* the F-coverage from 28% to less than 1% using electron beam irradiation. A significant change in the resistivity of FG has been shown to accompany this transition. It was found that the relative decrease in resistance per square upon electron irradiation of microstructures is at least seven orders of magnitude from 1 TΩ to 100 kΩ. Furthermore, our process can be used for patterning different surface areas ranging from few tens of squared micrometres to channels just a few tens of nanometres wide (dependent on e-beam resolution).

In summary, the patterning of fluorine-functionalization content in FG by means of electron beam irradiation offers novel avenues for biosensing. Sensing of various biological analytes has already been demonstrated using FG where the F content was varied. The implementation of FG biosensors where the F content is tuned by electron beam patterning to different values across the same device would enable new multifunctional biosensors whereby a wide variety of biomolecules can be detected in a single device, perhaps for the monitoring of biologically important analytes such as those needed for the management of diabetes and cardiovascular diseases (i.e. glucose, cholesterol, triglyceride, glycated haemoglobin).

Data accessibility. This article has no additional data.

Authors' contributions. All authors contributed significantly to this work. A.de.S., S.R., M.F.C. and C.D.W. wrote the paper. S.R., M.F.C. and C.D.W. led the work.

Competing interests. We declare we have no competing interests.

Funding. A.A., V.K.N., M.F.C. and C.D.W. acknowledge funding via the EU FP7 project CareRAMM (grant no. 309980). S.R. and M.F.C. acknowledge financial support from the Engineering and Physical Sciences Research Council (grant nos. EP/J000396/1, EP/K017160/1, EP/K010050/1, EP/G036101/1, EP/M001024/1 and EP/M002438/1).

References

1. Reina G, González-Domínguez JM, Criado A, Vázquez E, Bianco A, Prato M. 2017 Promises, facts and challenges for graphene in biomedical applications. *Chem. Soc. Rev.* **46**, 4400–4416. (doi:10.1039/C7CS00363C)
2. Song J, Yang X, Jacobson O, Lin L, Huang P, Niu G, Ma Q, Chen X. 2015 Sequential drug release and enhanced photothermal and photoacoustic effect of hybrid reduced graphene oxide-loaded ultrasmall gold nanorod vesicles for cancer therapy. *ACS Nano* **9**, 9199–9209. (doi:10.1021/acsnano.5b03804)
3. Liu Z, Robinson JT, Sun X, Dai H. 2008 PEGylated nanographene oxide for delivery of water-insoluble cancer drugs. *J. Am. Chem. Soc.* **130**, 10 876–10 877. (doi:10.1021/ja803688x)
4. Huang YS, Lu YJ, Chen J-P. 2017 Magnetic graphene oxide as a carrier for targeted delivery of chemotherapy drugs in cancer therapy. *J. Magn. Magn. Mater.* **427**, 34–40. (doi:10.1016/j.jmmm.2016.10.042)
5. Han X, Fang X, Shi A, Wang J, Zhang Y. 2013 An electrochemical DNA biosensor based on gold nanorods decorated graphene oxide sheets for sensing platform. *Anal. Biochem.* **443**, 117–123. (doi:10.1016/j.ab.2013.08.027)
6. Lee J, Park IS, Jung E, Lee Y, Min D-H. 2014 Direct, sequence-specific detection of dsDNA based on peptide nucleic acid and graphene oxide without requiring denaturation. *Biosens. Bioelectron.* **62**, 140–144. (doi:10.1016/j.bios.2014.06.028)
7. Sun L, Hu N, Peng J, Chen L, Weng J. 2014 Ultrasensitive detection of mitochondrial DNA mutation by graphene oxide/DNA hydrogel electrode. *Adv. Funct. Mater.* **24**, 6905–6913. (doi:10.1002/adfm.201402191)
8. Wang Y, Li Z, Hu D, Lin CT, Li J, Lin Y. 2010 Aptamer/graphene oxide nanocomplex for in situ molecular probing in living cells. *J. Am. Chem. Soc.* **132**, 9274–9276. (doi:10.1021/ja103169v)
9. Hu W, Peng C, Luo W, Ly M, Li X, Li D, Huang Q, Fan C. 2010 Graphene-based antibacterial paper. *ACS Nano* **4**, 4317–4323. (doi:10.1021/nn101097v)
10. Huang Y, Wang T, Zhao X, Wang X, Zhou L, Yang Y, Liao F, Ju Y. 2015 Poly(lactic acid)/graphene oxide-ZnO nanocomposite films with good mechanical, dynamic mechanical, anti-UV and antibacterial properties. *J. Chem. Technol. Biotechnol.* **90**, 1677–1684. (doi:10.1002/jctb.4476)
11. Marta B, Potara M, Iliut M, Jakab E, Radu T, Imre-Lucaci F, Katona G, Popescu O, Astilean S. 2015 Designing chitosan-silver nanoparticles-graphene oxide nanohybrids with enhanced antibacterial activity against *Staphylococcus aureus*. *Colloids Surf. A Physicochem. Eng. Asp.* **487**, 113–120. (doi:10.1016/j.colsurfa.2015.09.046)
12. Georgakilas V, Otyepka M, Bourlinos AB, Chandra V, Kim N, Kemp KC, Hobza P, Zboril R, Kim KS. 2012 Functionalization of graphene: covalent and non-covalent approaches, derivatives and applications. *Chem. Rev.* **112**, 6156–6214. (doi:10.1021/cr3000412)
13. Khrapach I, Withers F, Bointon TH, Polyushkin DK, Barnes WL, Russo S, Craciun MF. 2012 Novel highly conductive and transparent graphene-based conductors. *Adv. Mater.* **24**, 2844–2849. (doi:10.1002/adma.201200489)
14. Boopathi S, Narayanan TN, Kumar SS. 2014 Improved heterogeneous electron transfer kinetics of fluorinated graphene derivatives. *Nanoscale* **6**, 10 140–10 146. (doi:10.1039/C4NR02563F)
15. Kang J, Shin D, Bae S, Hong BH. 2012 Graphene transfer: key for applications. *Nanoscale* **4**, 5527–5537. (doi:10.1039/c2nr31317k)
16. Gong C, McDonnell S, Qin X, Azcatl A, Dong H, Chabal YJ, Cho K, Wallace RM. 2014 Realistic metal–graphene contact structures. *ACS Nano* **8**, 642–649. (doi:10.1021/nn405249n)
17. Robinson JA, LaBella M, Zhu M, Hollander M, Kasarda R, Hughes Z, Trumbull K, Cavalero R, Snyder D. 2011 Contacting graphene. *Appl. Phys. Lett.* **98**, 053103. (doi:10.1063/1.3549183)
18. Nourbakhsh A, Cantoro M, Vosch T, Pourtois G, Clemente F, van der Veen MH, Hofkens J, Heyns MM, de Gendt S, Sels BF. 2010 Bandgap opening in oxygen plasma-treated graphene. *Nanotechnology* **21**, 435203. (doi:10.1088/0957-4484/21/43/435203)
19. Aria AI, Gani AW, Gharib M. 2014 Effect of dry oxidation on the energy gap and chemical composition of CVD graphene on nickel. *Appl. Surf. Sci.* **293**, 1–11. (doi:10.1016/j.apsusc.2013.11.117)
20. Felten A, Flavel BS, Britnell L, Eckmann A, Louette P, Pireaux JJ, Hirtz M, Krupke R, Casiraghi C. 2013 Single- and double-sided chemical functionalization of bilayer graphene. *Small* **9**, 631–639. (doi:10.1002/smll.201202214)
21. Alexeev AM, Barnes MD, Nagareddy VK, Craciun MF, Wright CD. 2017 A simple process for the fabrication of large-area CVD graphene based devices via selective *in situ* functionalization and patterning. *2D Mater.* **4**, 011010. (doi:10.1088/2053-1583/4/1/011010)
22. Dreyer DR, Park S, Bielawski CW, Ruoff RS. 2010 The chemistry of graphene oxide. *Chem. Soc. Rev.* **39**, 228–240. (doi:10.1039/B917103G)
23. Mehrotra P. 2016 Biosensors and their applications. A review. *J. Oral Biol. Craniofac. Res.* **6**, 153–159. (doi:10.1016/j.jobcr.2015.12.002)
24. El-Zohary SE, Azzazi A, Okamoto H, Okamoto T, Haraguchi M, Swillam MA. 2013 Resonance-based integrated plasmonic nanosensor for lab-on-chip applications. *J. Nanophotonics* **7**, 073077. (doi:10.1117/1.JNP.7.073077)
25. Lapsley MI, Chiang I-K, Zheng YB, Ding X, Mao X, Huang TJ. 2011 A single-layer, planar, optouidic MachZehnder interferometer for label-free detection. *Lab Chip* **11**, 1795–1800. (doi:10.1039/c0lc00707b)
26. Simpson ML *et al.* 2001 An integrated CMOS microluminometer for low-level luminescence sensing in the bioluminescent bioreporter integrated circuit. *Sens. Actuators B* **72**, 134–140. (doi:10.1016/S0925-4005(00)00641-9)
27. Silva LB, Veigas B, Doria G, Costa P, Inacio J, Martins R, Fortunato E, Baptista PV. 2011 Portable optoelectronic biosensing platform for identification of mycobacteria from the *Mycobacterium tuberculosis* complex. *Biosens. Bioelectron.* **26**, 2012–2017. (doi:10.1016/j.bios.2010.08.078)
28. Ajami S, Teimouri F. 2015 Features and application of wearable biosensors in medical care. *J. Res. Med. Sci.* **20**, 1208–1215. (doi:10.4103/1735-1995.172991)
29. Neves AIS, Bointon TH, Melo LV, Russo S, de Schrijver I, Craciun MF, Alves H. 2015 Transparent conductive graphene textile fibers. *Sci. Rep.* **5**, 9866. (doi:10.1038/srep09866)
30. Neves AIS *et al.* 2017 Towards conductive textiles: coating polymeric fibres with graphene. *Sci. Rep.* **7**, 4250. (doi:10.1038/s41598-017-04453-7)
31. Wehenkel DJ, Bointon TH, Booth T, Boggild P, Craciun MF, Russo S. 2015 Unforeseen high temperature and humidity stability of $FeCl_3$ intercalated few layer graphene. *Sci. Rep.* **5**, 7609. (doi:10.1038/srep07609)
32. Bointon TH, Jones GF, De Sanctis A, Hill-Pearce R, Craciun MF, Russo, S. 2015 Large-area functionalized CVD graphene for work function matched transparent electrodes. *Sci. Rep.* **5**, 16464. (doi:10.1038/srep16464)
33. Bointon TH, Russo S, Craciun MF. 2015 Is graphene a good transparent electrode for photovoltaics and display applications? *IET Circuits Devices Syst.* **9**, 403–412. (doi:10.1049/iet-cds.2015.0121)
34. Torres Alonso E, Karkera G, Jones GF, Craciun MF, Russo S. 2016 Homogeneously bright, flexible, and foldable lighting devices with functionalized graphene electrodes. *ACS Appl. Mater. Interfaces* **8**, 16 541–16 545. (doi:10.1021/acsami.6b04042)
35. Craciun MF, Khrapach I, Barnes MD, Russo S. 2013 Properties and applications of chemically functionalized graphene. *J. Phys. Condens. Matter* **25**, 423201. (doi:10.1088/0953-8984/25/42/423201)
36. Efetov DK, Kim P. 2010 Controlling electron-phonon interactions in graphene at ultrahigh carrier densities. *Phys. Rev. Lett.* **105**, 256805. (doi:10.1103/PhysRevLett.105.256805)
37. Lemme MC, Koppens FHL, Falk AL, Rudner MS, Park H, Levitov LS, Marcus CM. 2011 Gate-activated photoresponse in a graphene p-n junction. *Nano Lett.* **11**, 4134–4137. (doi:10.1021/nl2019068)
38. Song JCW, Reizer MY, Levitov LS. 2012 Disorder-assisted electron-phonon scattering and cooling pathways in graphene. *Phys. Rev. Lett.* **109**, 106602. (doi:10.1103/PhysRevLett.109.106602)
39. Liu C-H, Chang Y-C, Norris TB, Zhong Z. 2014 Graphene photodetectors with ultrabroadband and high responsivity at room temperature. *Nat. Nanotechnol.* **9**, 273–278. (doi:10.1038/nnano.2014.31)
40. Tielrooij JK *et al.* 2015 Generation of photovoltage in graphene on a femtosecond timescale through efficient carrier heating. *Nat. Nanotechnol.* **10**, 437–443. (doi:10.1038/nnano.2015.54)

41. Wang L *et al.* 2013 One-dimensional electrical contact to a two-dimensional material. *Science* **342**, 614–617. (doi:10.1126/science.1244358)
42. Withers F, Bointon TH, Craciun MF, Russo S. 2013 All-graphene photodetectors. *ACS Nano* **7**, 5052–5057. (doi:10.1021/nn4005704)
43. De Sanctis A, Jones GF, Wehenkel DJ, Bezares F, Koppens FHL, Craciun MF, Russo S. 2017 Extraordinary linear dynamic range in laser-defined functionalized graphene photodetectors. *Sci. Adv.* **3**, e1602617. (doi:10.1126/sciadv.1602617)
44. De Sanctis A, Barnes MD, Amit I, Craciun MF, Russo S. 2017 Functionalised hexagonal domain graphene for position-sensitive photodetectors. *Nanotechnology* **28**, 124004. (doi:10.1088/1361-6528/aa5ec0)
45. Keilmann F, Hillenbrand R. 2004 Near-field microscopy by elastic light scattering from a tip. *Phil. Trans. R. Soc. Lond. A* **362**, 787–805. (doi:10.1098/rsta.2003.1347)
46. Valencia PM, Farokhzad OC, Karnik R, Langer R. 2012 Microfluidic technologies for accelerating the clinical translation of nanoparticles. *Nat. Nanotechnol.* **7**, 623–629. (doi:10.1038/nnano.2012.168)
47. Urbanová V *et al.* 2016 Fluorinated graphenes as advanced biosensors—effect of fluorine coverage on electron transfer properties and adsorption of biomolecules. *Nanoscale* **8**, 12 134–12 142. (doi:10.1039/C6NR00353B)
48. Chia X, Ambrosi A, Otyepka M, Zbořil R, Pum M. 2014 Fluorographites (CFx)n exhibit improved heterogeneous electron-transfer rates with increasing level of fluorination: towards the sensing of biomolecules. *Chemistry* **20**, 6665–6671. (doi:10.1002/chem.201402132)
49. Tadi KK, Pal S, Narayanan TN. 2016 Fluorographene based ultrasensitive ammonia sensor. *Sci. Rep.* **6**, 25221. (doi:10.1038/srep25221)
50. Zhang H, Fan L, Dong H, Zhang P, Nie K, Zhong J, Li Y, Guo J, Sun X. 2016 Spectroscopic investigation of plasma-fluorinated monolayer graphene and application for gas sensing. *ACS Appl. Mater. Interfaces* **8**, 8652–8661. (doi:10.1021/acsami.5b11872)
51. Chen M, Qiu C, Zhou H, Yang H, Fang Y, Sun L. 2013 Fluorination of edges and central areas of monolayer graphene by SF_6 and CHF_3 plasma treatments. *J. Nanosci. Nanotechnol.* **13** 1331–1334. (doi:10.1166/jnn.2013.5996)
52. Tahara K, Iwasaki T, Matsutani A, Hatano M. 2012 Asymmetric transport property of fluorinated graphene. *Appl. Phys. Lett.* **101**, 163105. (doi:10.1063/1.4760268)
53. Ho K, Liao J, Huang C, Hsu C, Zhang W Lu A-Y, Li L-J, Lai C-S, Su C-Y. 2014 One-step formation of a single atomic-layer transistor by the selective fluorination of a graphene film. *Small* **10**, 989–997. (doi:10.1002/smll.201301366)
54. Withers F, Bointon TH, Dubois M, Russo S, Craciun MF. 2011 Nanopatterning of fluorinated graphene by electron beam irradiation. *Nano Lett.* **11**, 3912–3916. (doi:10.1021/nl2020697)
55. Martins SE, Withers F, Dubois M, Craciun MF, Russo S. 2013 Tuning the transport gap of functionalized graphene via electron beam irradiation. *New J. Phys.* **15**, 033024. (doi:10.1088/1367-2630/15/3/033024)